



## **PPPL Reports Disclaimer**

This report was prepared as an account of work sponsored by an agency of the United States Government. Neither the United States Government nor any agency thereof, nor any of their employees, makes any warranty, express or implied, or assumes any legal liability or responsibility for the accuracy, completeness, or usefulness of any information, apparatus, product, or process disclosed, or represents that its use would not infringe privately owned rights. Reference herein to any specific commercial product, process, or service by trade name, trademark, manufacturer, or otherwise, does not necessarily constitute or imply its endorsement, recommendation, or favoring by the United States Government or any agency thereof. The views and opinions of authors expressed herein do not necessarily state or reflect those of the United States Government or any agency thereof.

## **Availability**

This report is posted on the U.S. Department of Energy's Princeton Plasma Physics Laboratory Publications and Reports web site in Fiscal Year 2003. The home page for PPPL Reports and Publications is: [http://www.pppl.gov/pub\\_report/](http://www.pppl.gov/pub_report/)

DOE and DOE Contractors can obtain copies of this report from:

U.S. Department of Energy  
Office of Scientific and Technical Information  
DOE Technical Information Services (DTIS)  
P.O. Box 62  
Oak Ridge, TN 37831

Telephone: (865) 576-8401

Fax: (865) 576-5728

Email: [reports@adonis.osti.gov](mailto:reports@adonis.osti.gov)

This report is available to the general public from:

National Technical Information Service  
U.S. Department of Commerce  
5285 Port Royal Road  
Springfield, VA 22161

Telephone: 1-800-553-6847 or  
(703) 605-6000

Fax: (703) 321-8547

Internet: <http://www.ntis.gov/ordering.htm>

# Self-consistent equilibrium model of low aspect-ratio toroidal plasma with energetic beam ions

E. V. Belova, N. N. Gorelenkov, and C. Z. Cheng

*Princeton Plasma Physics Laboratory, Princeton, New Jersey 08543*

A theoretical model is developed which allows the self-consistent inclusion of the effects of energetic beam ions in equilibrium calculations of low-aspect-ratio toroidal devices. A two-component plasma is considered, where the energetic ions are treated using a kinetic Vlasov description, while a one-fluid magnetohydrodynamic description is used to represent the thermal plasma. The model allows for an anisotropic distribution function and a large Larmor radius of the beam ions. Numerical results are obtained for neutral-beam-heated plasmas in the National Spherical Torus Experiment (NSTX). Self-consistent equilibria with an anisotropic fast ion distribution have been calculated for NSTX. It is shown for typical experimental parameters that the contribution of the energetic neutral beam ions to the total current can be comparable to that of the background plasma, and that the kinetic modifications of the equilibrium can be significant. The range of validity of the finite-Larmor-radius expansion and of the reduced kinetic descriptions for the beam ions in NSTX is discussed. The calculated kinetic equilibria can be used for self-consistent numerical studies of beam-ion-driven instabilities in NSTX.

# I. INTRODUCTION

Neutral Beam Injection (NBI) is commonly used as an effective way to heat and sustain plasma in a variety of magnetic confinement concepts. The presence of energetic neutral beam ions can significantly modify both the equilibrium and stability properties of toroidal plasmas, particularly in very low aspect-ratio toroidal devices, where the Alfvén velocity can be smaller than the injection velocity of the NBI ions. The relatively weaker toroidal field in these devices also results in a large Larmor radius of the energetic ions, which can be a significant fraction of the minor radius of the device. Unlike in a conventional large-aspect-ratio tokamak, the gyro-radius of the fast ions can be comparable to typical plasma scale lengths, which brings into question the validity of reduced kinetic descriptions (e.g., drift-kinetic) for the energetic ions. Therefore, new theoretical models are required, that do not rely on the finite Larmor radius (FLR) expansion. In this work, we develop an equilibrium model which allows the self-consistent inclusion of the effects of the energetic ions in calculations of low-aspect-ratio toroidal plasma equilibria. Particularly, equilibria of Spherical Tori (ST) are considered, and numerical results are obtained for neutral-beam-heated plasmas in the National Spherical Torus Experiment (NSTX).

In this paper, the plasma is assumed to consist of two components, the thermal background plasma, for which a one-fluid magnetohydrodynamic (MHD) description is used, and the energetic beam ion component, which is treated using a kinetic Vlasov description. A generalized form of the Grad-Shafranov equation is derived, which includes the effects of the beam ion toroidal and poloidal currents. It is assumed that the fast ion density is small compared to the total plasma density, but that the fast ion current and pressure can be com-

parable to that of the thermal plasma. The equilibrium electric field and the background plasma rotation are neglected in the present work.

An anisotropic distribution function is assumed for the beam ions, with  $\rho_b \sim L_n$ , where  $\rho_b$  is the beam ion gyroradius, and  $L_n$  is the density gradient scale length. These assumptions correspond to the experimental conditions in NSTX<sup>1</sup>, where the fast ion Larmor radius can be as large as one-third of the minor radius, and a strong anisotropy in the NBI ion pitch-angle distribution has been measured<sup>2</sup>. The NSTX is a low-aspect-ratio toroidal device with geometrical center major and minor radii,  $R_g = 0.85\text{m}$  and  $a = 0.65\text{m}$ , respectively. In NSTX, the magnetic field is low, and the NBI ion injection velocity is 2 to 4 times larger than the Alfvén speed<sup>1</sup>. The supra-Alfvénic fast ions can drive Alfvén modes unstable, and the anisotropy in the particle distribution<sup>3,4</sup>, as well as its spatial gradient provide the free energy source for these instabilities. Therefore, it is necessary to develop methods of calculating self-consistent equilibria for realistic beam ion distributions, when beam ion beta is comparable to background beta.

In this paper, a description of the numerical scheme for calculating such equilibria, and the results of the calculations are presented. It is shown that for typical NSTX experimental parameters, the contribution of the energetic neutral beam ions to the total current can be comparable to that of the background plasma, and the kinetic modifications of the equilibrium can be significant. The range of validity of the finite-Larmor-radius expansion and the drift-kinetic description for the beam ions in NSTX is discussed. The calculated kinetic equilibria can be used for a comparison with commonly-used one-fluid Grad-Shafranov equilibria, and they also have been used for self-consistent numerical studies of beam-ion-driven instabilities in NSTX<sup>5</sup>.

The outline of this paper is as follows. In Sec. II, the theoretical model is discussed, and the generalized Grad-Shafranov equation is derived. The form of the fast ion distribution function,  $F_0$ , and various approximations for the ion invariants of motion are considered in Sec. III. In Sec. IV, the calculation of the moments of  $F_0$  is presented, and a comparison is made between the drift-kinetic and the fully kinetic descriptions. Numerical methods for computing the equilibria with fast ions, and the results of these calculations are presented in Secs. V and VI. The summary and conclusions are presented in Sec. VII.

## II. GENERAL FORM OF GRAD-SHAFRANOV EQUATION

An equation describing the axisymmetric equilibrium of the two-component plasma (the thermal plasma plus the beam ions) can be obtained from the following set of equations:

$$0 = -\nabla p_p + (\mathbf{J} - \mathbf{J}_b) \times \mathbf{B}, \quad (1)$$

$$\mathbf{J} = \nabla \times \mathbf{B}, \quad (2)$$

$$0 = \nabla \cdot \mathbf{J}_b, \quad (3)$$

$$\mathbf{B} = \nabla \phi \times \nabla \psi + h \nabla \phi, \quad (4)$$

where the subscript “p” is used for thermal (fluid) plasma, and  $p_p$  is the fluid pressure. The subscript “b” is used to denote the beam ion density  $n_b$ , the beam ion generated current  $\mathbf{J}_b$ , etc.; the total current density is  $\mathbf{J} = \mathbf{J}_p + \mathbf{J}_b$ . Equation (1) is the momentum equation for the thermal plasma, where the equilibrium rotation has been neglected [ $\mathbf{V}_p = 0$ ]. The beam density is assumed to be small compared to the bulk density,  $n_b \ll n_e$ , therefore the MHD Ohm’s law applies, and the equilibrium electric field is also neglected i. e.,  $\mathbf{E} = 0$ . All quantities in Eqs. (1)-(4) are dimensionless, such that velocity is normalized to the Alfvén speed  $V_A = B_0/\sqrt{4\pi m_i n_0}$ , length is normalized to  $V_A/\omega_{ci}$ , where  $\omega_{ci} = q_i B_0/m_i c$ , and

the magnetic field and plasma density are normalized to the vacuum magnetic field at the geometrical center,  $B_0$ , and the peak electron density,  $n_0$ , respectively.

The Grad-Shafranov equation can be obtained from the toroidal component of the Ampere's law Eq. (2), using the flux representation for the poloidal magnetic field Eq. (4). This gives

$$R \frac{\partial}{\partial R} \left( \frac{1}{R} \frac{\partial \psi}{\partial R} \right) + \frac{\partial^2 \psi}{\partial Z^2} = R J_\phi, \quad (5)$$

where the standard cylindrical coordinate system  $(R, \phi, Z)$  is used, and  $\psi$  is the poloidal magnetic flux function, and in Eq. (4)  $h = RB_\phi$ .

In order to cast Eq. (5) into a more useful form, we need to express the total toroidal current  $J_\phi$  in terms of  $p_p$ ,  $h$ , and the beam ion current using the bulk plasma momentum equation. Since  $\nabla p_p$  has no component along the magnetic field, the bulk plasma pressure is a function of  $\psi$ , and  $\nabla p_p = p'_p \nabla \psi$ . Then from Eqs. (1), (2) and (4) it can be shown that

$$(R p'_p + J_\phi - J_{\phi,b}) \nabla \psi = -h (\nabla h / R + \mathbf{J}_{pol,b} \times \hat{\phi}), \quad (6)$$

where the prime denotes the differentiation with respect to the poloidal flux, and  $J_{\phi,b}$  and  $\mathbf{J}_{pol,b}$  are the toroidal and poloidal components of the beam current. It follows that

$$\mathbf{B} \cdot \nabla h = \mathbf{J}_{pol,b} \cdot \nabla \psi. \quad (7)$$

Therefore  $h$  is not a function of  $\psi$ , unless the beam ion poloidal current is zero, or it is parallel to the magnetic flux surface, which, in general, is not the case. From the fast ion continuity equation we have  $\nabla \cdot \mathbf{J}_{pol,b} = 0$ , and the fast ion poloidal current can be written in terms of the poloidal stream function  $G$  as

$$\mathbf{J}_{pol,b} = \nabla G \times \nabla \phi. \quad (8)$$

Now it can be shown that  $\mathbf{B} \cdot \nabla(h - G) = 0$ , and the function  $H \equiv h - G$  is a function of the poloidal flux. Substituting  $h = H(\psi) + G$  into Eq. (6), we can write the toroidal current as  $J_\phi = -Rp'_p - (H + G)H'/R + J_{\phi,b}$ .

The generalized Grad-Shafranov equation becomes

$$R \frac{\partial}{\partial R} \left( \frac{1}{R} \frac{\partial \psi}{\partial R} \right) + \frac{\partial^2 \psi}{\partial Z^2} = -R^2 p'_p - HH' - GH' + RJ_{\phi,b}. \quad (9)$$

The first two terms on the right-hand-side of Eq. (9) correspond to the usual MHD terms, whereas the last two terms are due to the fast ions. The equilibrium can be calculated if two magnetic surface functions  $p_p(\psi)$  and  $H(\psi)$  are specified, and the beam ion current is calculated using the fast ion distribution function  $F_0$ . The poloidal stream function  $G$  can be determined using Eq. (8).

### III. FAST ION DISTRIBUTION FUNCTION

Any integrable function of the particle invariants of motion can serve as a solution to the Vlasov equation. In this Section, we consider a suitable set of the phase-space variables, and present a model form of the fast ion distribution function  $F_0$ , which provides reasonable agreement with the experimental measurements.

#### A. Magnetic moment conservation

Assuming zero equilibrium electric field and an axisymmetric configuration, the fast ion constants of motion are the energy  $\varepsilon = v^2/2$ , the toroidal canonical angular momentum  $p_\phi = -\psi + (m_i c/q_i) R v_\phi$ , and the magnetic moment  $\mu$ . While the first two invariants are conserved exactly, the magnetic moment is an adiabatic invariant, which is based on the asymptotic expansion with respect to the parameter  $\epsilon_B \equiv \rho_i/L_B$ , where  $\rho_i$  is the fast ion Larmor radius, and  $L_B$  is the scale length of the background magnetic field variation. In

lowest order,  $\mu_0 = v_{\perp}^2/2B$ . Including the first-order corrections<sup>6-8</sup>, the magnetic moment is:

$$\mu = \mu_0 + \frac{\mu_0}{B}(\boldsymbol{\rho} \cdot \nabla B) + \frac{v_{\parallel}^2}{B}(\hat{\mathbf{b}} \cdot \nabla) \hat{\mathbf{b}} \cdot \boldsymbol{\rho} - \frac{\mu_0 v_{\parallel}}{2\Omega} [\hat{\mathbf{b}} \cdot \nabla \times \hat{\mathbf{b}} - 2(\hat{\mathbf{a}} \cdot \nabla \hat{\mathbf{b}}) \cdot \hat{\mathbf{c}}], \quad (10)$$

where  $\hat{\mathbf{b}}$  is a unit vector along the equilibrium magnetic field,  $\hat{\mathbf{c}} = \mathbf{v}_{\perp}/v_{\perp}$  and  $\hat{\mathbf{a}} = \hat{\mathbf{b}} \times \hat{\mathbf{c}}$  are unit vectors along the particle perpendicular velocity and the Larmor radius vector respectively,  $\boldsymbol{\rho}$  is the Larmor radius vector,  $\Omega = q_i B/m_i c$  is the local ion cyclotron frequency, and all fields are calculated at the particle position  $\mathbf{x}$ . Note that in the test particle calculations<sup>9</sup>, usually it is sufficient to know that an expression for  $\mu$ , conserved to the required accuracy, exists, but the explicit form for  $\mu$  is not needed. In self-consistent calculations, when the moments of the particle distribution function are calculated, an explicit relation between the particle variable phase-space  $(\mathbf{x}, \mathbf{v})$  and  $\mu$  is required, like the one given in Eq. (10).

We have used the hybrid and MHD simulation code (HYM)<sup>5</sup> to follow the fast particle orbits in the equilibrium field for a representative NSTX equilibrium. The conservation of the particle energy, the toroidal angular momentum, and the magnetic moment was monitored for several particle trajectories with  $v = 2.5V_A$ . For numerical efficiency, the expression for  $\mu$  in Eq. (10) has been modified, and the magnetic moment has been calculated as follows:

$$\mu = \left[ \frac{(\mathbf{v}_{\perp} - \mathbf{v}_d)^2}{2B} - \frac{v_{\parallel}}{2B} \mathbf{v}_{\perp} \cdot \hat{\mathbf{b}}(\mathbf{x} - \boldsymbol{\rho}) \right] \left( 1 - \frac{v_{\parallel}}{2\Omega} \hat{\mathbf{b}} \cdot \nabla \times \hat{\mathbf{b}} \right), \quad (11)$$

where  $\mathbf{v}_d = \mu_0 \hat{\mathbf{b}} \times \nabla B/\Omega + v_{\parallel}^2 \hat{\mathbf{b}} \times (\hat{\mathbf{b}} \cdot \nabla) \hat{\mathbf{b}}/\Omega$  is the magnetic gradient and curvature drift velocity, and the unit vector  $\hat{\mathbf{b}}(\mathbf{x} - \boldsymbol{\rho})$  in the square brackets is evaluated at the guiding-center position  $\mathbf{X} = \mathbf{x} - \boldsymbol{\rho}$ . This expression for  $\mu$  agrees with Eq. (10) to order  $O(\epsilon_B)$ , and includes some of the higher-order corrections.

Figure 1 shows a typical particle orbit projected on the poloidal plane, and Fig. 2 shows the variation of the normalized particle energy,  $p_{\phi}$ ,  $\mu_0$ , and  $\mu = \mu_0 + \mu_1$  along this orbit.

The relative amplitudes of the change in  $\mu_0$  and  $\mu$  are  $\sim 30\%$  and  $< 4\%$  respectively, while  $\varepsilon$  and  $p_\phi$  conservation is exact within the numerical accuracy. Other orbits, with the same particle energy and different pitch angles, show variation of  $\mu_0$  by more than 60% of its value, whereas the expression in Eq. (11) is conserved to within 10%. It is evident that the lowest order magnetic moment  $\mu_0$  is a very poor approximation for the fast ions in NSTX, while the higher-order corrections provide considerably better accuracy. Non-conservation of  $\mu$ , caused by resonances between particle bounce motion and its gyromotion, may lead to a stochastic particle transport<sup>10</sup>. Since these resonances are typically of high order [ $> 10$ ], non-adiabatic variations of  $\mu$  can be neglected for our purposes.

## B. Guiding-center variables

Since  $\mu$  is a good invariant, the equilibrium distribution function can be taken as  $F_0 = F_0(\varepsilon, p_\phi, \mu)$ . The calculation of the moments of  $F_0$  can be simplified by using a transformation from the particle variables  $(\mathbf{x}, \mathbf{v})$  to the guiding-center variables  $(\mathbf{X}, U, \mu, \theta)$ , where  $\mathbf{X}$  is the guiding-center position,  $U$  is the parallel velocity, and  $\theta$  is the gyro-angle. Such a transformation can be constructed, for example, by using Hamiltonian (Lie transforms) methods, as was done by Littlejohn<sup>6,7</sup>. In the guiding-center variables, the particle phase space is four-dimensional due to the axial symmetry and the independence of  $F_0$  upon the gyro-angle (by construction).

For 80keV deuterium NBI ions in NSTX, the value of the small parameter  $\epsilon_B$  can be estimated as  $\epsilon_B \approx \rho_i/R_0 \lesssim 0.2$ . As our test particle simulations have shown, an expansion with respect to  $\epsilon_B$ , and therefore, the guiding-center description of the particle orbits is valid, but the first-order corrections must be included. In addition to Eq. (10), the relations between the guiding-center and particle variables are given by<sup>6</sup>

$$\mathbf{X} = \mathbf{x} - \boldsymbol{\rho} + O(\epsilon_B^2) \quad (12)$$

$$U = v_{\parallel} - v_{\parallel}(\hat{\mathbf{b}} \cdot \nabla) \hat{\mathbf{b}} \cdot \boldsymbol{\rho} + \frac{\mu_0 B}{2\Omega} [\hat{\mathbf{b}} \cdot \nabla \times \hat{\mathbf{b}} - 2(\hat{\mathbf{a}} \cdot \nabla \hat{\mathbf{b}}) \cdot \hat{\mathbf{c}}] \quad (13)$$

while the expression for  $\theta$  is not needed here. Due to the choice of transformation which preserves the form of the guiding-center Hamiltonian, we have  $\varepsilon = v_{\parallel}^2/2 + \mu_0 B(\mathbf{x}) = U^2/2 + \mu B(\mathbf{X}) + O(\epsilon_B^2)$ .

The toroidal angular momentum in guiding-center coordinates is calculated in Appendix A, where it is shown that

$$p_{\phi} = -\psi + \bar{\varepsilon} U R b_{\phi} - \bar{\varepsilon}^2 \mu [b_z + R b_{\phi} (\hat{\mathbf{b}} \cdot \nabla \times \hat{\mathbf{b}})/2] + O(\epsilon_B^2), \quad (14)$$

where  $\bar{\varepsilon} \equiv m_i c/q_i$ , and fields are calculated at the guiding-center position. The formal orders of the three terms on the right-hand-side of Eq. (14) are  $O(1/\epsilon_B)$ ,  $O(1)$ , and  $O(\epsilon_B)$ , respectively. In lowest order,  $p_{\phi} = -\psi(\mathbf{x})$ , which is the common large-aspect-ratio tokamak approximation. In next order,  $p_{\phi} = -\psi(\mathbf{X}) + \bar{\varepsilon} U R b_{\phi}$ , where  $\mathbf{X} = \mathbf{x} - \boldsymbol{\rho}$  is the guiding-center position. The first term in Eq. (14) is formally  $O(1/\epsilon_B)$  [due to the  $B = O(1)$  ordering] therefore, the calculation of  $p_{\phi}$  through first-order requires the second-order corrections for  $\mathbf{X}$ . This is further discussed in the Appendix A.

Figure 3 shows the time evolution of  $p_{\phi}$  under three different approximations. The values of  $p_{\phi}$  are calculated along the same particle trajectory, as shown in Fig. 1. It is evident that  $p_{\phi} \approx -\psi(\mathbf{x})$  is not suitable for the fast ions in NSTX, because a change in the value of the poloidal flux along the particle orbit can be of the order of  $|\psi_0|$ . The next-order correction, Fig. 3(b), provides much better accuracy; however, for some orbits, the variation in  $p_{\phi} = -\psi(\mathbf{X}) + \bar{\varepsilon} U R b_{\phi}$  has been found to be up to 30%. In contrast, the expression given in Eq. (14) has been found to be nearly as accurate as that of the exact form [Fig. 2(b)].

The advantage of the guiding-center representation, Eq. (14), is that in this representation  $p_\phi$  is explicitly gyro-angle independent.

### C. Equilibrium distribution function

Realistic distribution function can be obtained by the Monte-Carlo simulations, like one implemented in TRANSP code<sup>11</sup>. In NSTX, neutral beams are injected tangentially to a major radius, so in many applications the pitch angle distribution can be approximated by Gaussian distribution. Therefore, in this paper, the equilibrium distribution function is taken to be of the form  $F_0 = F_1(v)F_2(\lambda)F_3(p_\phi, v, \lambda)$ , where  $v = \sqrt{2\varepsilon}$  is the particle velocity,  $\lambda \equiv \mu B_0/\varepsilon$  is the pitch-angle variable, and the functions  $F_{1,2,3}$  are defined by

$$F_1(v) = \frac{1}{v^3 + v_*^3}, \quad \text{for } v < v_0, \quad (15)$$

$$F_2(\lambda) = C \exp(-(\lambda - \lambda_0)^2/\Delta\lambda^2), \quad (16)$$

$$F_3(p_\phi, v, \lambda) = \frac{(p_\phi - p_{\min})^\alpha}{(p_{\max} - p_{\min})^\alpha}, \quad \text{for } p_\phi > p_{\min}(v, \lambda), \quad (17)$$

where  $F_0 = 0$  for  $v > v_0$  or  $p_\phi < p_{\min}(v, \lambda)$ . Thus,  $F_0$  is assumed to be a slowing-down distribution in  $v$ , where  $v_0 \approx 3.5V_A$  is the injection velocity, and  $v_* = v_0/2$ , which correspond to typical NSTX parameters. The pitch-angle distribution is assumed to be relatively narrow with  $\Delta\lambda = 0.3$  at large  $v$ ;  $\lambda_0$  is taken to be between 0.5 and 0.8; and  $C$  is a normalization constant. The function  $F_3(p_\phi, v, \lambda)$  is used to match the profiles of the beam ion density calculated by TRANSP, where  $\alpha$  is a numerical parameter [ $\alpha = 2$  or  $4$ ], and the condition  $p_\phi > p_{\min}(v, \lambda)$  describes a prompt-loss boundary. The denominator in the expression for  $F_3$  is used for proper velocity space normalization.

#### 1. Prompt-loss boundary and $p_\phi$ dependence

The form of  $p_{\min}(v, \lambda)$  can be found from prompt orbit-loss condition in the guiding-

center variables<sup>12,13</sup>. Assuming  $p_\phi \approx -\psi + \bar{\epsilon}URb_\phi$ , the particle guiding-center orbit with constant  $p_\phi$ ,  $v$ , and  $\lambda$  can be described in the  $(\xi, \psi)$  plane by the relation  $\psi = -p_\phi \pm \bar{\epsilon}vh(\psi)/B_0\sqrt{\xi(\xi - \lambda)}$ , where  $\xi = B_0/B$  [with  $B=B(R,0)$  taken at the equatorial plane  $z=0$ ],  $B_0$  is the vacuum magnetic field at the geometric center, and  $h = RB_\phi$  has been defined in Sec. II. The tip of the projection of the particle orbit into  $(\xi, \psi)$  plane corresponds to a point  $(\xi = \lambda, \psi = -p_\phi)$ . Thus, for a given particle energy, there is a unique correspondence between the particle phase-space  $(\lambda, p_\phi)$  and the orbit representation in the  $(\xi, \psi)$  plane<sup>12</sup>.

Considering a class of the particle orbits crossing the plasma boundary at the equatorial plane, the confinement region can be described approximately by  $p_\phi > p_{\min}$ , where

$$p_{\min}(v, \lambda) = \begin{cases} p_1 = \bar{\epsilon}vh(0)/B_0\sqrt{\xi_{\max}(\xi_{\max} - \lambda)}, & \text{for } \lambda > \xi_c, \\ p_2 = -\psi(\xi = \lambda), & \text{for } \xi_{\min} < \lambda < \xi_c, \\ p_3 = -\bar{\epsilon}vh(0)/B_0\sqrt{\xi_{\min}(\xi_{\min} - \lambda)}, & \text{for } \lambda < \xi_{\min}. \end{cases}$$

Here we assume that  $\psi = 0$  at the plasma boundary,  $\xi_{\max}$  and  $\xi_{\min}$  are maximum and minimum values of  $\xi$  at the outermost flux surface, and  $\xi = \xi_c$  at the intersection of the trapped-passing boundary  $p_2$  and the trapped-particle loss boundary  $p_1$ .

The prompt-loss boundaries have been studied for a representative NSTX equilibrium with maximum beta 26%, and  $q_0 = 1.15$ . The phase-space topologies for two values of the particle energy corresponding to  $v = 2V_A$  and  $v = 3V_A$  are shown in Figs. 4(a) and 4(b). The curves defined by the relations  $p_\phi = p_1$ ,  $p_\phi = p_2$ , and  $p_\phi = p_3$  are labeled as 1, 2, and 3, respectively. Curve 1 describes the tips of the trapped orbits passing through  $(\xi_{\max}, \psi = 0)$  for the positive sign of  $U$ ; curve 2 is approximately the trapped-passing boundary; and curve 3 corresponds to the tips of the counter-passing orbits ( $U < 0$ ) passing through  $(\xi_{\min}, \psi = 0)$ .

The phase-space is bounded by  $p_\phi \leq p_{\max}(v, \lambda)$ , above which no orbit can exist. This

boundary is described approximately by curves 4 and 5 [Fig. 4]. Curve 4 [4'] corresponds to orbits passing through the magnetic axis, so that  $p_\phi = -\psi_0 \pm \bar{e}vR_0\sqrt{1 - \lambda/\xi_0}$  with positive [negative] sign, where  $\psi_0$  and  $R_0$  are the poloidal flux and the radius at the axis, and  $\xi_0 = \xi(R_0)$ . Curve 5 corresponds to  $p_\phi = -\psi(\xi = \lambda)$ .

Note that the expression for  $p_{\min}$  and the phase-space boundaries plotted in Fig. 4 have been obtained using the guiding center description of the fast ion orbits. Figure 4 also shows scatter plots of the particle distribution in phase space, which have been obtained from the full-orbit test particle simulations using the HYM code. In these simulations, the test particles have been loaded initially with a uniform distribution in the configuration space and a given energy [i.e. delta-function distribution  $\delta(v - v_0)$ ], corresponding to  $v_0 = 2V_A$  [Fig. 4(a)] or  $v_0 = 3V_A$  [Fig. 4(b)]. Only particles which remained confined after  $t = 300(1/\omega_{ci})$  have been plotted.

It is evident that guiding-center description of the prompt loss boundaries is accurate for lower particle energies with  $v \lesssim 2V_A$ , but the agreement is not as good for the ions with  $v \sim 3V_A$ . The discrepancy is largest at the trapped-orbit-loss boundary (curve 1), and for  $\lambda \gtrsim 1$ . One of the sources of inaccuracy is an FLR effect related to the difference between the particle position and its guiding center position. It has been taken into account by shifting curve 1 along the  $\lambda$ -axis by the value of the normalized Larmor radius at the plasma edge  $\sim \rho_i/R_0$ , which is shown by curves labeled 1' in Figs. 4(a) and 4(b). A fraction of trapped orbits (confined) has been found to be sensitive to the equilibrium profiles, in particular  $h(\psi)$  profile. For  $v \lesssim 2V_A$  and  $\lambda_0 \gtrsim 0.7$ , the fraction of trapped particles can be larger than that of the passing particles.

An interesting feature of the  $v = 3V_A$  case is a gap in the particle phase-space at low

$\lambda$ , between curves 1' and 4' as shown in Fig. 4(b). It occurs because there are no confined orbits for the particle parameters in the region of the phase space formed by the intersection of the curves 1' and 4' [this region corresponds to co-passing prompt loss orbits]. As a result, co-passing and counter-passing confined orbits are completely separated in the  $(p_\phi, \lambda)$  plane for  $v = 3V_A$ . For lower values of the fast ion energy ( $v \leq 2V_A$ ), the curves 1' and 4' do not intersect, and there is partial overlap of the confined co- and counter-passing orbits in phase space [Fig. 4(a)].

For numerical purposes, the expressions for  $p_{\min}$  and  $p_{\max}$  can be simplified. Assuming the co-injection,  $0.5 \lesssim \lambda_0 \lesssim 1$ , and a relatively narrow distribution in the pitch-angle parameter  $\lambda$ , the prompt-loss boundary,  $p_{\min}$ , and  $p_{\max}$  in Eq. (17) can be approximated by

$$p_{\min} = \bar{\epsilon} v h(0) \sqrt{\xi_{\max} (\xi_{\max} - \lambda_0) / B_0}, \quad (18)$$

$$p_{\max} = -\psi_0 + \bar{\epsilon} R_0 v \sqrt{1 - \lambda_0 / \xi_{\max}}. \quad (19)$$

## 2. Pitch-angle dependence $F_2(\lambda)$

Distribution function of deuterium NBI ions, calculated by TRANSP code for NSTX shot #108236 at  $t = 0.151$ sec, is shown in Fig. 5(a), where  $v_{\parallel}$  and  $v_{\perp}$  denote particle velocities parallel and perpendicular to the equilibrium magnetic field, normalized to the injection velocity  $v_0$ . In this example, the distribution function has been averaged over the minor radius  $r$  for  $0.5a < r < 0.6a$  at the low-field-side, and averaged over  $v$  at low energies. In order to match an analytical distribution function  $F_0$  given by Eqs. (15)-(17) locally to that from TRANSP calculations, the dependence of the width of the pitch-angle distribution  $F_2(\lambda)$  on the particle energy has to be taken into account. The effect of the strong pitch-angle scattering at low energies can be modeled according to<sup>14,15</sup>

$$\Delta\lambda^2 = \Delta_0^2 - A(1 - \lambda_0) \ln \left[ \frac{v^3(1 + v_*^3/v_0^3)}{v^3 + v_*^3} \right], \quad (20)$$

where  $\Delta_0$  is the width of the  $\lambda$ -distribution at large  $v$ , and  $A$  is a numerical parameter used to match the TRANSP results. For  $\Delta\lambda$  dependent on the particle energy, the normalization coefficient in Eq. (16) needs to be chosen as

$$C(v) = \frac{2}{\sqrt{\pi}\Delta\lambda} [\text{Erf}((1 - \lambda_0)/\Delta\lambda) + \text{Erf}(\lambda_0/\Delta\lambda)]^{-1},$$

where Erf is the error-function. Figure 5(b) shows the contour plot of  $F_0$ , calculated at  $r = 0.5a$  [low-field-side], and for the following set of parameters:  $\lambda_0 = 0.6$ ,  $\Delta_0 = 0.3$ ,  $A = 1/3$  and  $\alpha = 4$ . It is seen that the analytical distribution function reproduces major features of the TRANSP calculation. [Note that TRANSP code assumes conservation of the lowest-order magnetic moment,  $\mu_0$ , therefore, an exact comparison of distribution function  $F_0$  with that calculated by TRANSP, is not possible.]

#### IV. CALCULATION OF THE MACROSCOPIC MOMENTS OF $F_0$

The solution of the generalized Grad-Shafranov equation Eq. (9) requires calculation of the energetic ion poloidal and toroidal currents. The beam ion density is also needed for a comparison with the corresponding TRANSP profiles. Therefore, we need to calculate the moments of  $F_0$

$$n_b = \int F_1(v)F_2(\lambda, \Delta\lambda)F_3(p_\phi, p_{\min}, p_{\max}) d^3\mathbf{v}, \quad (21)$$

$$\mathbf{J}_b = \int \mathbf{v}F_1(v)F_2(\lambda, \Delta\lambda)F_3(p_\phi, p_{\min}, p_{\max}) d^3\mathbf{v}, \quad (22)$$

where  $\Delta\lambda$ ,  $p_{\min}$ , and  $p_{\max}$  are the functions of  $v$  given by Eqs. (18)-(20). The finite poloidal current of the fast ions results from the pitch-angle dependence of  $F_0$ , i. e.,  $\mathbf{J}_{pol,b} \neq 0$  provided  $\partial F_2/\partial\lambda \neq 0$ . In this Section, we calculate moments of  $F_0$  using the drift-kinetic

approximation, which relies on the FLR expansion of  $F_0$ . The moments of  $F_0$  are also calculated directly, as given by Eqs. (21) and (22), in order to examine the validity of the FLR expansion.

It is known<sup>16</sup> that current of the energetic beam ions  $J_{\parallel,b}$  excites an oppositely directed electron-drag current  $-J_{\parallel,b}(Z_b/Z_{eff})$  for beam energies  $E > (m_i/m_e)^{1/3}T_e$ . As a result, the parallel component of the beam-ion-generated current is modified by a factor  $(1 - Z_b/Z_{eff})$ , where  $Z_{eff}$  is the effective plasma charge. This effect is important for alpha particles, and it can result in a cancellation or even reversion of the alpha-particle-generated current compared to the pure alpha-particle current. For NBI ions in NSTX however, the ratio  $Z_b/Z_{eff}$  is estimated as  $\approx 1/3$ , therefore this effect is not expected significantly modify the equilibrium, and it has been neglected in this paper.

## A. Drift-kinetic approximation

As shown in Appendix B, the fast ion density and current density can be calculated as

$$n_b(\mathbf{x}) = \int F_0 B_{\parallel}^* dU d\mu, \quad (23)$$

$$\mathbf{J}_b(\mathbf{x}) = \int (U \hat{\mathbf{b}} + \mathbf{V}_d) F_0 B_{\parallel}^* dU d\mu + \nabla \times \mathbf{M}, \quad (24)$$

where  $B_{\parallel}^* = B(1 + U/\Omega \hat{\mathbf{b}} \cdot \nabla \times \hat{\mathbf{b}})$  is the Jacobian of the transformation to guiding-center variables,  $\mathbf{V}_d = \mu \hat{\mathbf{b}} \times \nabla B / \Omega + U^2 \hat{\mathbf{b}} \times (\hat{\mathbf{b}} \cdot \nabla) \hat{\mathbf{b}} / \Omega$  is the magnetic gradient and curvature drift velocity, and  $\mathbf{M} = -\hat{\mathbf{b}} \int (\mu B / \Omega) F_0 B dU d\mu$  is the magnetization vector. Equations (23) and (24) have been obtained by making a transformation to guiding-center variables in Eqs. (21) and (22), and using the FLR expansion of  $F_0$  according to  $F_0(\mathbf{x} - \boldsymbol{\rho}) \approx F_0(\mathbf{x}) - \boldsymbol{\rho} \cdot \nabla F_0 + O(\epsilon^2)$ . The small parameter for this expansion is  $\epsilon \equiv \rho_i / L_n$ , which is the ratio of the fast ion Larmor radius to the perpendicular scale length of the fast ion density gradient. For

NSTX,  $\epsilon > \epsilon_B$ .

We define the guiding center fluid moments [the density, parallel current, parallel and perpendicular pressures] by  $N = \int F_0 B dU d\mu$ ,  $NV_{\parallel} = \int U F_0 B dU d\mu$ ,  $P_{\parallel} = \int U^2 F_0 B dU d\mu$ , and  $P_{\perp} = \int \mu F_0 B^2 dU d\mu$ , respectively. Then, in terms of the guiding center fluid moments, the fast ion density and current density can be written as

$$n_b(\mathbf{x}) = N + NV_{\parallel}(\hat{\mathbf{b}} \cdot \nabla \times \hat{\mathbf{b}})/\Omega + O(\epsilon^2), \quad (25)$$

$$\mathbf{J}_b(\mathbf{x}) = NV_{\parallel} \hat{\mathbf{b}} + (P_{\parallel} - P_{\perp})\nabla \times \hat{\mathbf{b}}/\Omega + \hat{\mathbf{b}} \times \nabla P_{\perp}/\Omega + O(\epsilon^2). \quad (26)$$

The perpendicular part of the beam ion current can be easily recognized as the diamagnetic current with the pressure tensor taken in the Chew-Goldberger-Low [CGL] form.

It has been shown in Sec. II, that contributions of the fast ions in the generalized Grad-Shafranov equation appear in terms of the toroidal component of the fast ion current, and the poloidal stream function  $G$  defined by Eq. (8). For a chosen form of the fast ion distribution function  $F_0$ , the expression for  $G$  can be found analytically using Eq. (24). The poloidal component of the magnetization current can be written as  $(\nabla \times \mathbf{M})_{pol} = \nabla(RM_{\phi}) \times \nabla\phi$ . Therefore,  $\mathbf{J}_{pol,b} = \nabla(\tilde{G} + RM_{\phi}) \times \nabla\phi$ , where  $G = \tilde{G} + RM_{\phi}$ , and  $M_{\phi} = -\int(\mu B_{\phi}/\Omega)F_0 B dU d\mu$ . The equation for  $\tilde{G}$  then becomes

$$\begin{aligned} \nabla\tilde{G} &= \int \left[ -U\nabla\psi + m_i c/q_i (U^2\nabla(Rb_{\phi}) - Rb_{\phi}\mu\nabla B) \right] F_0 dU d\mu \\ &= \int [U\nabla p_{\phi} - m_i c/q_i Rb_{\phi}\nabla\epsilon] F_0 dU d\mu, \end{aligned}$$

where  $\hat{\phi} \times \mathbf{B} = -\nabla\psi/R$ , and  $\hat{\phi} \times (\nabla \times \hat{\mathbf{b}}) = \nabla(Rb_{\phi})/R$  have been used. Changing variables from  $(U, \mu)$  to  $(\epsilon, \mu)$ , and using  $U\nabla|_{\epsilon,\mu} p_{\phi} = U\nabla|_{U,\mu} p_{\phi} - m_i c/q_i Rb_{\phi}\nabla|_{U,\mu} \epsilon$  [the gradients are taken with fixed  $\epsilon, \mu$  or with fixed  $U, \mu$ ], we obtain

$$\nabla \tilde{G} = \int (\nabla|_{\varepsilon, \mu} p_\phi) F_0 d\varepsilon d\mu = \nabla \int \hat{F}_0 d\varepsilon d\mu. \quad (27)$$

The solution is  $\tilde{G} = \int \hat{F}_0 d\varepsilon d\mu$ , where  $\hat{F}_0$  is a function of  $(\varepsilon, \lambda, p_\phi)$  which satisfies  $\partial \hat{F}_0 / \partial p_\phi = F_0$ . From Eq. (17), we find  $\hat{F}_0 = (p_\phi - p_{\min}) F_0 / (\alpha + 1)$ . The poloidal stream function of the fast ions then becomes

$$G = \int \left[ \frac{U(p_\phi - p_{\min})}{\alpha + 1} - \mu R B_\phi m_i c / q_i \right] F_0 dU d\mu. \quad (28)$$

Integrating by parts, it can also be shown that  $G = - \int \lambda (\partial \hat{F}_0 / \partial \lambda)|_{\varepsilon, p_\phi} d\varepsilon d\mu$ , which demonstrates a relation between the poloidal current and the pitch-angle dependence of  $F_0$ .

## B. Fully kinetic calculations

The Larmor radius of the NBI ions in NSTX can be as large as one-third of the minor radius, therefore for peaked beam ion profiles with  $L_n < a$ , we have  $\epsilon > 0.3$ , and the accuracy of the FLR expansion needs to be examined. The major difficulties in calculating the fast ion density and current directly from Eqs. (21) and (22) are that the first-order corrections for the magnetic moment must be explicitly included, and that the velocity space becomes three-dimensional. Using a local coordinate system specified by the unit vectors  $\hat{\mathbf{e}}_1 = \hat{\mathbf{b}}$ ,  $\hat{\mathbf{e}}_2 = \hat{\mathbf{b}} \times \hat{\mathbf{z}} / \sqrt{1 - b_z^2}$ , and  $\hat{\mathbf{e}}_3 = \hat{\mathbf{b}} \times \hat{\mathbf{e}}_2$ , we have  $d^3\mathbf{v} = dv_1 dv_2 dv_3$ ,  $\mu_0 = (v_2^2 + v_3^2) / 2B$ ,  $\rho = (v_2 \hat{\mathbf{e}}_3 - v_3 \hat{\mathbf{e}}_2) / \Omega$ , etc. In this basis, the expression for  $\mu$  becomes:

$$\mu = \left[ \frac{(\mathbf{v}_\perp - \mathbf{v}_d)^2}{2B} + \frac{v_1}{4B\Omega} \left\{ (v_2^2 - v_3^2) a_{23} - 2v_2 v_3 a_{22} \right\} \right] \left( 1 - v_1 (\hat{\mathbf{b}} \cdot \nabla \times \hat{\mathbf{b}}) / \Omega \right),$$

where the scalars  $a_{23}$  and  $a_{22}$  are defined as  $a_{23} = (\hat{\mathbf{e}}_2 \cdot \nabla \hat{\mathbf{b}}) \cdot \hat{\mathbf{e}}_3 + (\hat{\mathbf{e}}_3 \cdot \nabla \hat{\mathbf{b}}) \cdot \hat{\mathbf{e}}_2$ , and  $a_{22} = (\hat{\mathbf{e}}_2 \cdot \nabla \hat{\mathbf{b}}) \cdot \hat{\mathbf{e}}_2 - (\hat{\mathbf{e}}_3 \cdot \nabla \hat{\mathbf{b}}) \cdot \hat{\mathbf{e}}_3$ . It can be shown that  $a_{23} = -(\hat{\mathbf{b}} \cdot \nabla \times \hat{\mathbf{b}}) - 2\hat{\mathbf{e}}_2 \cdot \nabla b_z / \sqrt{1 - b_z^2}$ , and  $a_{22} = (\nabla \cdot \hat{\mathbf{b}}) + 2\hat{\mathbf{e}}_3 \cdot \nabla b_z / \sqrt{1 - b_z^2}$ .

In the general case, the poloidal stream function  $G$  cannot be determined analytically, therefore it has been calculated using the equation

$$R \frac{\partial}{\partial R} \left( \frac{1}{R} \frac{\partial G}{\partial R} \right) + \frac{\partial^2 G}{\partial Z^2} = -R \hat{\phi} \cdot \nabla \times \mathbf{J}_{pol,b}. \quad (29)$$

The fast ion density and current have been calculated for a typical NSTX equilibrium using both the drift-kinetic approximation [Eqs. (25)-(26)] and the integration of Eqs. (21) and (22). Figures 6(a) and 6(b) show the radial profiles of the beam ion toroidal current and the poloidal stream function, respectively, calculated for the following set of distribution function parameters:  $\lambda_0 = 0.8$ ,  $v_0 = 3.5V_A$ ,  $\alpha = 4$  and  $\Delta_0 = 0.3$ . The exact solution is shown by the solid lines, and the dashed lines show the drift-kinetic results. The position of the magnetic axis is shown by a vertical line. It is seen that drift-kinetic approximation results in a more peaked current profile, and it also overestimates the outward shift of the fast ion profiles relative to the magnetic flux surfaces. For injection velocity  $v_0 = 3.5V_A$ , the characteristic Larmor radius of the NBI ions  $\rho_b = v_0/\omega_{ci}$  is of order  $\rho_b \approx 0.2R_0$ , and the magnitude of the outward shift can be estimated as  $(1/3)\rho_b$  for the exact solution, and it is  $\sim (1/2)\rho_b$  for the drift-kinetic approximation.

The difference between the exact solution and the drift-kinetic approximation in Fig. 6(a) is of order  $\sim O(\epsilon^2)$ , and it depends strongly on the beam ion parameters, particularly on the values of  $v_0$  and  $\lambda_0$ . Figure 7 shows the magnitude of the second-order correction to the fast ion toroidal current  $\Delta J_{\phi,b} = b_\phi/2\nabla_\perp^2 \int (U\mu B/\Omega^2) F_0 B dU d\mu$  [calculated in Appendix B, Eq. (36)], for different values of the injection velocity and the pitch-angle parameter. This correction serves as a measure of the accuracy of the drift-kinetic description of the fast ion profiles. It is seen that the error in the drift-kinetic profiles can be as large as 30% for  $\lambda_0 = 0.8$  and  $v_0 \gtrsim 3.5V_A$ . The accuracy of the drift-kinetic description improves for smaller values of injection velocity or smaller values of  $\lambda_0$ .

Despite the low aspect-ratio in NSTX, the scale length of the magnetic field is significantly larger than that of the beam ion profiles. For our parameters, the ratio is about  $R_0/L_n \sim 2 - 3$ . Therefore, the validity of the  $\epsilon_B$ -expansion does not necessarily imply that an expansion with respect to  $\epsilon$  converges. As we have shown, the accuracy of Eqs. (25-26) depends on the peakedness of the fast ion profiles and the injection energy. For typical NBI parameters in NSTX, a higher-order FLR description, as given in Appendix B, or a fully kinetic description [Eqs. (21)-(22)] may be necessary.

### C. Effects of $\mu$ -corrections

It is interesting to examine the effects of the FLR corrections for  $\mu$  [Eq. (10)] on the fast ion current in Eq. (22). First, it can be shown that, if the lowest-order expression for the magnetic moment  $\mu_0 = v_{\perp}^2/2B$  is used, the beam current is parallel to the flux surface, and the poloidal stream function is a function of  $\psi$ . This can be shown by calculating

$$\hat{\mathbf{b}} \times \hat{\phi} \cdot \mathbf{J}_b = \int \mathbf{v} \times \hat{\mathbf{b}} \cdot \hat{\phi} F_0 d^3\mathbf{v} = \frac{q_i}{m_i c} \int \frac{\partial}{\partial \mathbf{v}} \cdot (\mathbf{v} \times \hat{\mathbf{b}} \hat{F}_0/R) d^3\mathbf{v} = 0,$$

where it was assumed that  $F_0$  depends on  $\lambda = \mu_0 B_0/\varepsilon$ . It then follows that  $\nabla\psi \cdot \mathbf{J}_b = 0$ , and that  $G = G(\psi)$ . Therefore, the first-order corrections for  $\mu$  qualitatively change the fast ion current profiles, namely, these corrections are responsible for a component of the fast ion current perpendicular to the flux surface.

Second, one of the checks of the calculated equilibria is the accuracy with which the calculated fast ion current [Eq. (22)] is divergence-free. This is particularly important if the calculated equilibrium is to be used as an initial condition for nonlinear simulations, which can be obscured by the equilibrium relaxation. If  $F_0$  satisfies the equilibrium Vlasov equation exactly, then Eq. (3) is exact. It is expected that when the magnetic moment is

approximated by  $\mu_0$ , the resulting current is divergence-free with  $O(\epsilon_B)$  accuracy, whereas with the higher-order corrections,  $\nabla \cdot \mathbf{J}_b = O(\epsilon_B^2)$ . For same parameters as in Fig. 6, we find  $\nabla \cdot \mathbf{J}_b \approx [0.4/R_0] \max(J_b)$  for zero-order  $\mu$ , and an order-of-magnitude smaller value is obtained when the higher-order corrections are retained.

## V. NUMERICAL SCHEME

The Grad-Shafranov equation Eq. (9) has been solved as a free-boundary problem, i.e., with the plasma-vacuum boundary found during the calculations. The solution has been obtained iteratively on a rectangular  $(R, Z)$  grid, and the boundary conditions and the profiles have been chosen to match the field and plasma profiles obtained from the TRANSP code. Without going into the details of the calculation of MHD equilibria [which can be found elsewhere<sup>17</sup>], in this Section we focus on including the fast ion effects into the equilibrium solver.

In Eq. (9), the flux-function  $H(\psi)$  has been assumed to be of the form  $H^2 = H_0^2(1 + \alpha_1 f_1(\psi) + \alpha_2 f_2(\psi))$ , where  $f_1$  and  $f_2$  are given functions of  $\psi$ , and the coefficients  $\alpha_1$  and  $\alpha_2$  are determined during Grad-Shafranov iterations from two constraints imposed on the solution. The first constraint requires that the total toroidal current  $I_\phi$  remains constant during the iterations. The second constraint is that the value of  $q$  (safety factor) at the magnetic axis is fixed at  $q = q_0$ . Since at the axis  $q \approx 2h/(R_0^2 J_\phi)$ , for the MHD case a relation between  $q_0$  and  $H$  and  $p$  functions is given by

$$q_0 = -\frac{2H(\psi_0)}{R_0(R_0^2 p'(\psi_0) + HH'(\psi_0))}. \quad (30)$$

The slowest part of the computation is the calculation of the integrals of the fast ion distribution function. This can be minimized by using two levels of iteration in Eq (9).

First, the MHD solution is found neglecting the fast ion current, and the calculated  $\psi$  and magnetic field are used to find  $\mathbf{J}_b$  from Eq. (22). The fast ion terms are then substituted into the right-hand-side of the Grad-Shafranov equation, and a new solution is computed for a given  $\mathbf{J}_b$ . The process is iterated until a convergence criterion is satisfied, which typically requires fewer than ten cycles.

In the calculations, it has been discovered that, when the condition  $2h/(R_0^2 J_\phi) = q_0$  is imposed at the magnetic axis, no convergent solution can be found. Therefore, an MHD expression, as in Eq. (30), has been used instead as the second constraint. As a result, the actual value of  $q$  at the axis obtained for equilibria with the fast ion component was smaller than that for the similar MHD solution [with the same  $I_\phi$ ]. The reduction was significant for larger beam density.

## VI. RESULTS

Self-consistent equilibria have been calculated for different fast ion parameters and densities up to  $n_b/n_0 = 0.1$ . The calculations have been performed starting from a reference MHD equilibrium with maximum thermal plasma beta  $\beta = 26\%$ , and  $q_0 = 1.15$ , assuming that  $n_e = 3.2 \cdot 10^{13} \text{cm}^{-3}$ ,  $B_0 = 3 \text{kG}$ , and the beam energy  $E = 80 \text{keV}$ , which corresponds to  $v_0 \approx 3.5V_A$ . The results of the calculations for  $n_b/n_0 = 0.05$  are shown in Fig. 8, where the contour plots of the poloidal cross section of the fast ion density and the components of current density  $\mathbf{J}_b$  are plotted. Figure 9 shows the corresponding radial profiles at the equatorial plane. The profile of  $q$  for this equilibrium is shown in Fig. 10.

The fast ion distribution function parameters have been taken  $\lambda_0 = 0.8$ ,  $\Delta\lambda = 0.3$ , and  $\alpha = 4$ . For this set of parameters, the magnitude of the peak beam current is about 20% of

the bulk current when  $n_b/n_0 = 0.03$ , and it increases to  $\sim 50\%$  for  $n_b/n_0 \gtrsim 0.05$ . Thus, even for modest NBI ion densities, the contribution of the beam ion current can be significant.

The fast ion pressure tensor is not needed for the solution of the generalized Grad-Shafranov equation Eq. (9), but it has been calculated as a diagnostic for a comparison with the fluid profiles. Figure 11(a) shows the components of the fast ion pressure tensor  $\mathbf{p}_b$  for the above distribution function parameters. Both the fluid and beam pressure are normalized to  $B_0^2/4\pi$ . It can be seen that the perpendicular component of  $\mathbf{p}_b$  is a factor of two larger than the parallel one for  $\lambda_0 = 0.8$ . The calculations show that the off-diagonal elements of the fast ion pressure tensor are comparable to  $p_{\parallel,b}$ . The radial profiles of the total and the bulk fluid pressure are shown in Fig. 11(b), where the total pressure has been defined as  $p_{tot} = p_p + (p_{\parallel,b} + 2p_{\perp,b})/3$ .

As can be seen from Figs. 8 and 11, the fast ion current and pressure profiles are relatively peaked, and they are also shifted outward relative to the magnetic flux surfaces. For large fast ion density, this results in a significant modification of the total [bulk plasma plus the beam ions] pressure and current profiles, especially on the low-field-side. Due to kinetic modifications, the resulting equilibrium is different from one-fluid MHD equilibria, since the total plasma pressure is strongly anisotropic and it is not a function of  $\psi$ .

Other major effects, resulting from the self-consistent inclusion of the NBI ion contribution, are the increase in the Shafranov shift, and the decrease of the value of the central  $q$  compared to the reference MHD equilibrium. The reduction in  $q_{axis}$  is likely to be caused by the peakedness of the NBI ion pressure profiles. Figure 12 shows the dependence of the position of the magnetic axis  $R_0$ , and the value of  $q_{axis}$  on the fast ion density. The calculations have been done for the same total toroidal current  $I_\phi$  and the fast ion parameters, but

varying the fast ion density. It is seen, that as  $n_b$  is increased to 8 % of the bulk density, the position of axis is changed by 5%, and value of  $q_{axis}$  drops significantly from  $q_{axis} = 1.15$  to 0.73.

It is known that at the high  $\beta$  and the high poloidal field in NSTX, a significant absolute magnetic well can be formed in the core region<sup>1</sup>. The reference MHD equilibrium used in this work has relatively low  $\beta$ , without the magnetic well. However, it has been found that, when effects of the NBI ions are added, the radial profile of the magnitude of the magnetic field flattens locally at  $R > R_0$ . Further increase in the beam density [in our case to 8%], resulted in a formation of the absolute minimum of  $B$  at low-field-side, which indicates that NBI can contribute to the formation of the magnetic well in the core for smaller bulk plasma beta.

## VII. SUMMARY AND CONCLUSIONS

A theoretical model has been developed which allows calculation of self-consistent equilibria for two-component plasma in small-aspect-ratio toroidal devices. The plasma is assumed to consist of the thermal background plasma, for which the one-fluid MHD description is used, and the low-density energetic ion component. The energetic ion contribution is included non-perturbatively, and the generalized Grad-Shafranov equation is derived, which includes the effects of the beam ion toroidal and poloidal currents.

An analytical form of the fast ion distribution function is presented, which takes into account prompt loss conditions, anisotropy, and the large Larmor radius of the beam ions. The distribution function computed for the 80 keV deuterium NBI ions in the NSTX compares favorably with TRANSP code calculations. Chosen distribution function can also be

used as a basis function, i. e. the set of basis functions of similar form [in our case, having different  $\lambda_0$ ] can represent any kind of measured or modeled general distribution function of beam ions.

Expressions for the fast ion current and poloidal stream function are derived using an FLR expansion of the fast ion distribution function. The range of validity of this expansion for NBI parameters in NSTX has been studied. It is shown that for smaller values of the pitch angle parameter, the drift-kinetic approximation provides a good description for the fast ion profiles, whereas for  $\lambda_0 \sim 1$  and injection velocity  $v_0 \gtrsim 3V_A$ , higher-order corrections or an exact integration of  $F_0$  are necessary.

Self-consistent equilibria including the NBI ion effects have been calculated numerically for neutral-beam-heated plasmas in NSTX. It is shown that for typical experimental parameters, kinetic modifications of the equilibrium profiles can be significant. In particular, the current profiles become more peaked, and the total plasma pressure is strongly anisotropic in the presence of a significant fast ion population. The main self-consistent effects of the NBI ions on equilibrium are an increase in the Shafranov shift, and a reduction of the  $q_{axis}$  value compared to the reference MHD equilibrium. NBI ions are also found to contribute to the formation of the local magnetic well inside plasma at the low-field-side.

The calculated kinetic equilibria can be used for a comparison with commonly used fluid equilibrium models, and they can serve as an initial condition for self-consistent numerical studies of the beam ion driven instabilities in NSTX. The model developed in this paper can also be used to study the effects of the energetic alpha particles on the equilibrium, for example, in deuterium-tritium ST reactor<sup>18</sup> with the correction for the alpha-induced electron current. The important effects of the NBI-induced rotation on the equilibrium

profiles have not been considered here, and will be included in future work.

## **ACKNOWLEDGMENTS**

This research was supported by the U.S. Department of Energy under Contract No. DE-AC02-76CH03073.

## APPENDIX A: HIGHER-ORDER CORRECTIONS FOR $P_\phi$

The angular momentum conservation in the guiding-center system was discussed in detail in Ref. 7. Since the system possesses azimuthal symmetry, then  $p_\phi = \bar{\epsilon} \partial L / \partial \dot{\phi}$  is a constant of the guiding-center motion, where  $L$  is the Lagrangian<sup>19</sup>

$$L = \left( \frac{1}{\bar{\epsilon}} \mathbf{A} + U \hat{\mathbf{b}} - \bar{\epsilon} \mu \left[ \mathbf{R} + \hat{\mathbf{b}} (\hat{\mathbf{b}} \cdot \nabla \times \hat{\mathbf{b}}) / 2 \right] \right) \cdot \dot{\mathbf{X}} + \bar{\epsilon} \mu \dot{\theta} - (U^2/2 + \mu B), \quad (31)$$

and  $\mathbf{A}$  is the vector potential,  $\bar{\epsilon} \equiv m_i c / q_i$ ,  $\mathbf{R} = \nabla \hat{e}_2 \cdot \hat{e}_3$ , where  $\hat{e}_2$  and  $\hat{e}_3$  are unit vectors perpendicular to the magnetic field, and we choose the same guiding-center transformation as in Refs. 6 and 19. Thus, the angular momentum in these guiding-center coordinates is given by

$$p_\phi = -\psi + \bar{\epsilon} U R b_\phi - \bar{\epsilon}^2 \mu [b_z + R b_\phi (\hat{\mathbf{b}} \cdot \nabla \times \hat{\mathbf{b}}) / 2]. \quad (32)$$

Just like  $\mu$ , the guiding-center angular momentum is exactly conserved by the guiding-center equations of motion correct to a given order. On the other hand, since the relations between the particle and guiding-center variables are known only up to  $O(\epsilon_B)$ , the expression in Eq. (32) is a first-order approximation for  $p_\phi$ .

The first term in Eq. (32) is formally  $O(1/\epsilon_B)$ , therefore, the calculation of  $p_\phi$  through first-order requires the second-order expression for  $\mathbf{X}$ . The higher-order relation between the guiding-center position and the particle position  $\mathbf{x}$  was calculated by Littlejohn<sup>7</sup>, and can be expressed as

$$\begin{aligned} \mathbf{X} = & \mathbf{x} - \boldsymbol{\rho} \\ & + \boldsymbol{\rho} \left[ \frac{v_{\parallel}}{\Omega} \hat{\mathbf{b}} \cdot \nabla \times \hat{\mathbf{b}} - \frac{1}{2B} \boldsymbol{\rho} \cdot \nabla B \right] + \hat{\mathbf{b}} \left[ \frac{2v_{\parallel} v_{\perp}}{\Omega^2} (\hat{\mathbf{b}} \cdot \nabla \hat{\mathbf{b}}) \cdot \hat{\mathbf{c}} + \frac{\mu_0 B}{4\Omega^2} \left( (\hat{\mathbf{c}} \cdot \nabla \hat{\mathbf{b}}) \cdot \hat{\mathbf{c}} - 5(\hat{\mathbf{a}} \cdot \nabla \hat{\mathbf{b}}) \cdot \hat{\mathbf{a}} \right) \right]. \end{aligned} \quad (33)$$

The last two terms in Eq. (33) are the second-order corrections, of which only the first is needed, since  $\hat{\mathbf{b}} \cdot \nabla \psi = 0$ .

## APPENDIX B: CALCULATION OF DENSITY INTEGRALS IN THE GUIDING CENTER VARIABLES

Here we derive an explicit expression for the fast ion current density integral in terms of the guiding center coordinates  $\mathbf{Z} = (\mathbf{X}, U, \mu, \theta)$ . An additional expansion parameter, which is related to the fast ion profile is  $\epsilon = \rho_i/L_n$ , where  $L_n = |\nabla_{\perp} n_b/n_b|^{-1}$  is the perpendicular density gradient scale length [from the guiding center Vlasov equation it follows that  $\rho_i \nabla_{\parallel} F_0/F_0 = O(\epsilon_B)$ ]. It is assumed that  $\epsilon \gg \epsilon_B$ .

The general expression for transformation of density integrals to guiding-center coordinates was given in Ref. 19, and the first-order expression, accurate to  $O(\epsilon, \epsilon_B)$ , was derived, for example, in Ref. 20. We calculate the fast ion current following Ref. 19 and keep higher-order terms in the  $\epsilon$ -expansion. Using the relations between the particle phase-space coordinates  $(\mathbf{x}, \mathbf{v})$  and the guiding-center coordinates, it can be shown that

$$\mathbf{J}_b(\mathbf{x}) = \int \mathbf{V}_{GC} F(\mathbf{Z}) \delta(\mathbf{X} + \boldsymbol{\rho}(\mathbf{X}) - \mathbf{x}) B_{\parallel}^* d^6 \mathbf{Z}, \quad (34)$$

where  $F(\mathbf{Z})$  is distribution function in guiding-center variables [in our case,  $F = F_0(\epsilon, p_{\phi}, \mu)$ , where values of  $\epsilon$ , and  $p_{\phi}$  do not change in the transformation], and  $B_{\parallel}^* = B(1 + U/\Omega \hat{\mathbf{b}} \cdot \nabla \times \hat{\mathbf{b}})$  is the Jacobian of the transformation. The velocity in guiding-center coordinates,  $\mathbf{V}_{GC} \equiv \mathbf{v}(\mathbf{Z})$ , can be written as<sup>19</sup>  $\mathbf{V}_{GC} = U \hat{\mathbf{b}} + \mathbf{V}_{\perp} + \mathbf{V}_d + \tilde{\mathbf{V}}_d$ . First two terms are the  $O(1)$  parallel and perpendicular velocities,  $\mathbf{V}_d = \mu \hat{\mathbf{b}} \times \nabla B/\Omega + U^2 \hat{\mathbf{b}} \times (\hat{\mathbf{b}} \cdot \nabla) \hat{\mathbf{b}}/\Omega$  is the magnetic gradient and curvature drift velocity, and  $\tilde{\mathbf{V}}_d = O(\epsilon_B)$  is the oscillating part [with zero gyroaverage].

Using the Larmor radius expansion everywhere, except in the distribution function, and keeping only the terms first-order in  $\epsilon_B$ , the current can be written as

$$\mathbf{J}_b(\mathbf{x}) = \int \left[ \mathbf{V}_{GC} B_{\parallel}^* - \left( U \nabla \cdot (\hat{\mathbf{b}} \times \mathbf{V}_{\perp} \hat{\mathbf{b}}) + \nabla \cdot (\hat{\mathbf{b}} \times \mathbf{V}_{\perp} \mathbf{V}_{\perp}) \right) \frac{B}{\Omega} \right] F_0(\mathbf{x} - \boldsymbol{\rho}, U, \mu) dU d\mu d\theta.$$

This expression is valid for  $\epsilon = O(1)$ , but no gyroaveraging can be done explicitly, because the arguments in  $F_0$  depend on the gyroangle. Assuming  $\epsilon \ll 1$ , and using the  $\epsilon_B = O(\epsilon^2)$  ordering, we obtain

$$\mathbf{J}_b(\mathbf{x}) = \int \left[ U \hat{\mathbf{b}} B_{\parallel}^* \langle F_0 \rangle + \mathbf{V}_d B_{\parallel}^* F_0 - \nabla \cdot \langle \hat{\mathbf{b}} \times \mathbf{V}_{\perp} \mathbf{V}_{\perp} \rangle B F_0 / \Omega + \langle \mathbf{V}_{\perp} F_0 \rangle B \right] dU d\mu, \quad (35)$$

where angular brackets denote the gyroaveraging, and  $O(\epsilon\epsilon_B)$  terms have been neglected. The gyroaverages are calculated as  $\langle F_0 \rangle = F_0 + \mu B \nabla_{\perp}^2 F_0 / 2\Omega^2$ ,  $\nabla \cdot \langle \hat{\mathbf{b}} \times \mathbf{V}_{\perp} \mathbf{V}_{\perp} \rangle = \mu \nabla \times \mathbf{B}$ , and  $\langle \mathbf{V}_{\perp} F_0 \rangle = \mu \mathbf{B} \times \nabla F_0 / \Omega$ . Therefore, the expression for the beam ion current becomes

$$\mathbf{J}_b(\mathbf{x}) = \int \left[ (U \hat{\mathbf{b}} + \mathbf{V}_d) B_{\parallel}^* F_0 - \mu \nabla \times (\mathbf{B} F_0) B / \Omega + \hat{\mathbf{b}} U \mu \nabla_{\perp}^2 F_0 B^2 / 2\Omega^2 \right] dU d\mu. \quad (36)$$

In the same way, the beam ion density can be written as

$$n_b(\mathbf{x}) = \int \left[ B_{\parallel}^* F_0 + \mu \nabla_{\perp}^2 F_0 B^2 / 2\Omega^2 \right] dU d\mu. \quad (37)$$

These expressions for the beam ion density and current rely on the  $\epsilon$ -expansion of the fast-ion distribution function, and are valid through order  $O(\epsilon_B)$  and  $O(\epsilon^2)$ . By neglecting the second-order terms in  $\epsilon$ , we obtain Eqs. (23) and (24) used in Sec. IV, which agrees with results obtained in Ref. 20.

- 
- <sup>1</sup> M. Ono, S. M. Kaye, Y.-K. M. Peng, et al., Nucl. Fusion **40**, 557 (2000).
- <sup>2</sup> S. S. Medley, private communication (2003).
- <sup>3</sup> N. N. Gorelenkov, C. Z. Cheng, and E. D. Fredrickson, Phys. Plasmas **9**, 3483 (2002).
- <sup>4</sup> E. D. Fredrickson, N. N. Gorelenkov, C. Z. Cheng, et al., Phys. Plasmas **9**, 2069 (2002).
- <sup>5</sup> E. V. Belova, N. N. Gorelenkov, C. Z. Cheng, R. C. Davidson, and E. D. Fredrickson, Bull. Am. Phys. Soc. **47**, 169 (2002).
- <sup>6</sup> R. G. Littlejohn, Phys. Fluids **24**, 1730 (1981).
- <sup>7</sup> R. G. Littlejohn, Plasma Physics **29**, 111 (1983).
- <sup>8</sup> M. D. Kruskal, J. Math. Phys. **3**, 806 (1962).
- <sup>9</sup> D. R. Mikkelsen, R. B. White, R. J. Akers, S. M. Kaye, D. C. McCune, and J. E. Menard, Phys. Plasmas **4**, 3667 (1997).
- <sup>10</sup> V. A. Yavorskij, D. Darrow, V. Ya. Goloborod'ko, S. N. Reznik, U. Holzmueller-Steinacker, N. Gorelenkov, and K. Schoepf, Nucl. Fusion **42**, 1210 (2002).
- <sup>11</sup> R. V. Budny, Nucl. Fusion **34**, 1247 (1994).
- <sup>12</sup> C. T. Hsu, and D. J. Sigmar, Phys. Fluids B **4**, 1492 (1992).
- <sup>13</sup> C. M. Doloc, and G. Martin, Nucl. Fusion **35**, 1543 (1995).
- <sup>14</sup> C. Angioni, A. Pochelone, N. N. Gorelenkov, et.al. Plasma Phys. Control. Fusion **44**, 205 (2002).

- <sup>15</sup> H. L. Berk, W. Horton, M. N. Rosenbluth and P. H. Rutherford, Nucl. Fusion **15**, 819 (1975).
- <sup>16</sup> Ya. I. Kolesnichenko, V. V. Parail, and G. V. Pereverzev, in *Reviews of Plasma Physics* edited by B. B. Kadomtsev (Consultants Bureau, New York, 1986), Vol. 17, p.48; S. V. Putvinskij, Vol. 18, p. 310.
- <sup>17</sup> J. L. Johnson, H. E. Dalhed, J. M. Greene, et al., J. Comput. Phys. **32**, 212 (1979); K. Lackner, Comput. Phys. Com. **12**, 33 (1976).
- <sup>18</sup> M. Peng, Phys. Plasmas **7**, 1681 (2000).
- <sup>19</sup> A. Brizard, Plasma Phys. **41**, 541 (1989).
- <sup>20</sup> I. B. Bernstein, and P. J. Catto, Phys. Fluids **28**, 1342 (1985).

## FIGURE CAPTIONS

FIG.1. Poloidal projection of the particle orbit with  $v = 2.5V_A$ ; dashed lines are the contours of poloidal flux.

FIG.2. Variation of the normalized particle energy,  $p_\phi$ ,  $\mu_0$ , and  $\mu$  along the orbit shown in Fig. 1.

FIG.3. Time evolution of  $p_\phi$  along the orbit shown in Fig. 1, calculated in three different approximations: (a)  $p_\phi = -\psi(\mathbf{x})$ , (b)  $p_\phi = -\psi(\mathbf{x} - \boldsymbol{\rho}) + (m_i c/q_i)RUb_\phi$ , and (c)  $p_\phi$  obtained from Eq. (14).

FIG.4. Phase-space topology of the particle orbits for (a)  $v = 2V_A$ , and (b)  $v = 3V_A$ ; curves 1, 2, 3, and 4' represent the prompt loss boundaries; scatter plots are obtained from full-orbit test particle simulations; and  $\lambda$  is defined by  $\lambda = \mu B_0/\varepsilon$ .

FIG.5. Distribution function of NBI ions from (a) TRANSP calculations for NSTX shot #108236 [ $t = 0.151\text{sec}$ ], and from (b) the analytical form of  $F_0$  given in Eqs. (15)-(17) and calculated at  $r = 0.5a$  at the low-field-side.

FIG.6. Radial profiles of (a) the beam ion toroidal current, and (b) the poloidal stream function. The exact results are shown by the solid lines, and the drift-kinetic approximations are shown by the dashed lines.

FIG.7. Magnitude of the second-order correction  $O(\epsilon^2)$  to the fast ion toroidal current calculated using the drift-kinetic approximation for different values of the injection velocity  $v_0$ , and the pitch-angle parameter  $\lambda_0$ .

FIG.8. Contour plots in the poloidal cross section of the fast ion (a) density, (b) toroidal current, (c) and (d) poloidal current. Contours of constant  $\psi$  are shown with dashed lines.

FIG.9. Radial profiles at the equatorial plane of the normalized (a) fast ion density, (b)

fast ion toroidal current, (c) fast ion poloidal current, and (d) total and bulk plasma toroidal current. Vertical lines indicate the position of the magnetic axis.

FIG.10. Plot of the  $q$  profile for the calculations shown in Figs. 9 and 10 with beam ion density  $n_b = 5\%$  (solid line), and  $q$  profile for MHD equilibrium (dashed line).

FIG.11. Radial profiles of (a) parallel and perpendicular components of the fast ion pressure, and (b) total pressure and fluid pressure for  $\lambda_0 = 0.8$  and  $n_b/n_0 = 0.05$ .

FIG.12. Dependence on the fast ion density of (a) the position of the magnetic axis  $R_0$ , and (b) the value of  $q_{axis}$ .

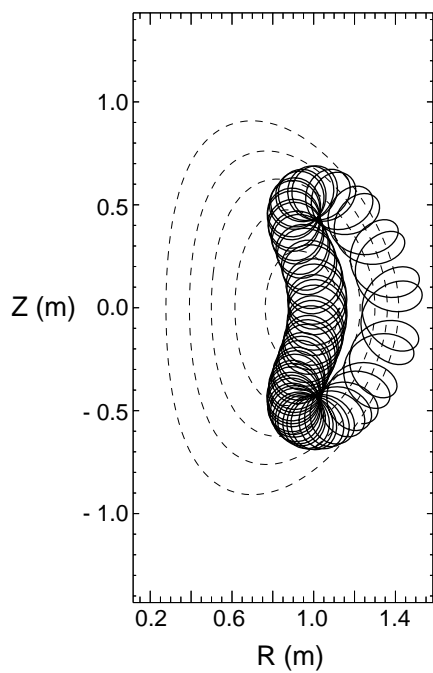


Figure 1.

Belova, Gorelenkov, Cheng

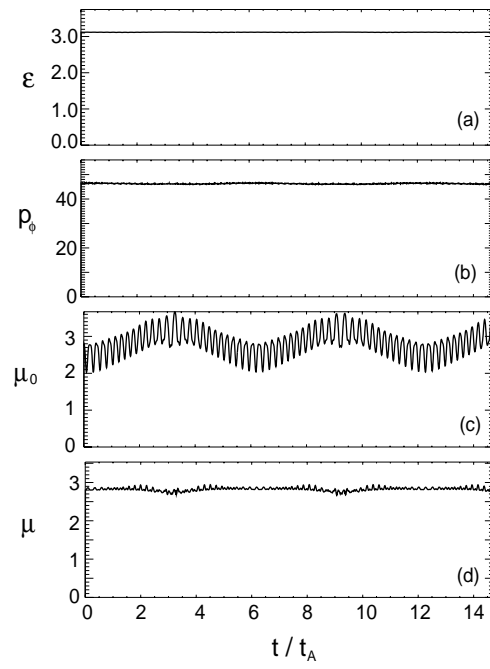


Figure 2.

Belova, Gorelenkov, Cheng

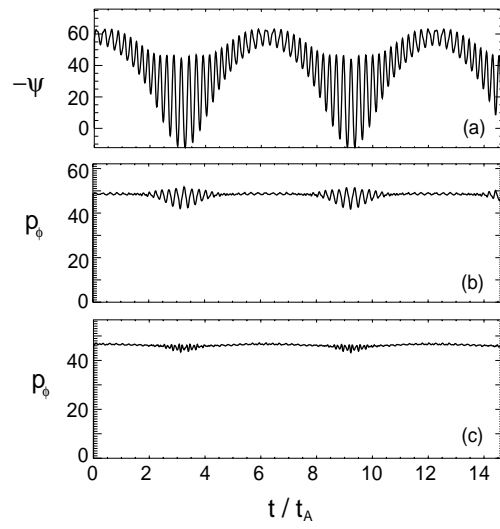


Figure 3.

Belova, Gorelenkov, Cheng

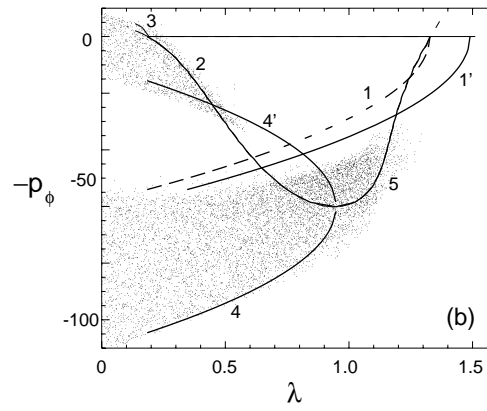
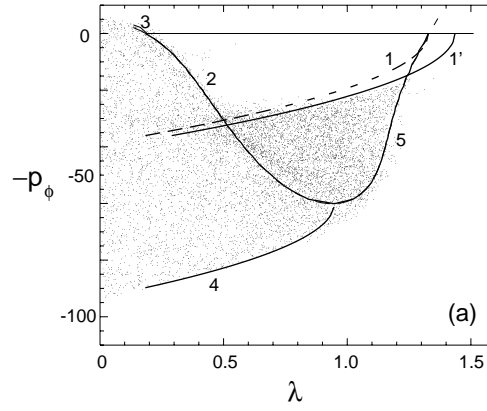


Figure 4.

Belova, Gorelenkov, Cheng

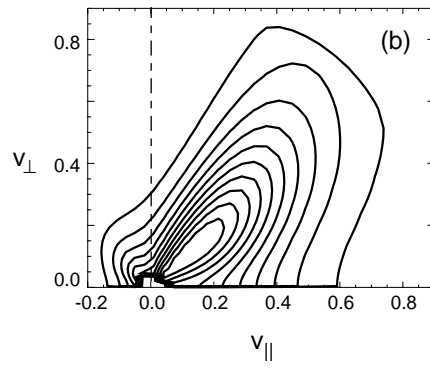
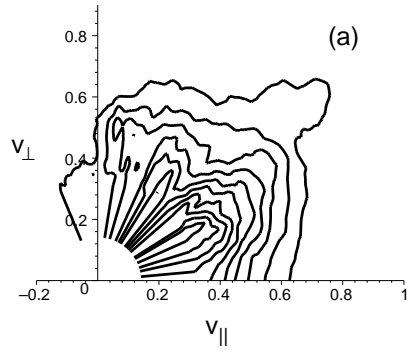


Figure 5.

Belova, Gorelenkov, Cheng

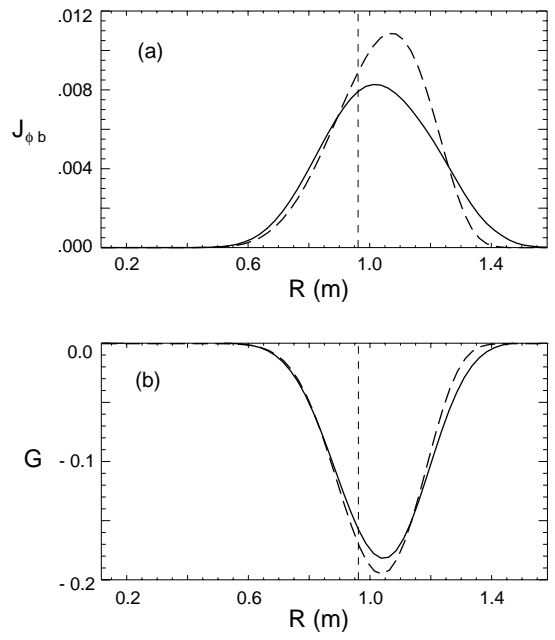


Figure 6.

Belova, Gorelenkov, Cheng

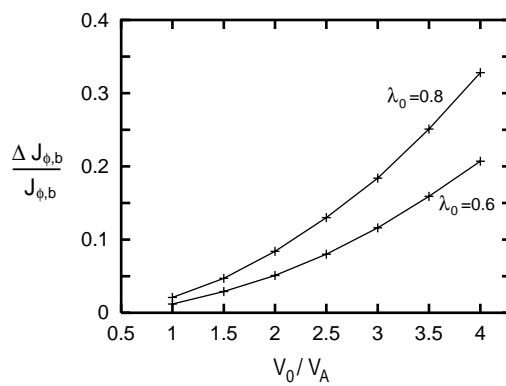


Figure 7.

Belova, Gorelenkov, Cheng

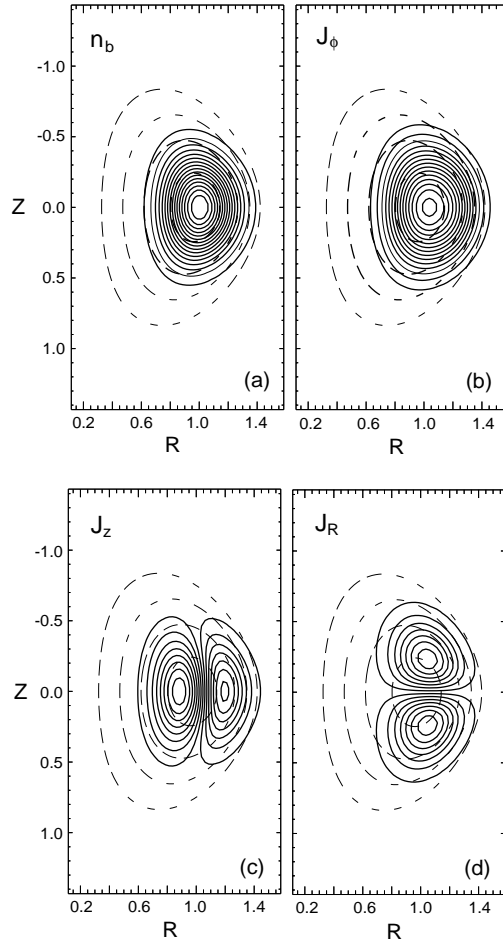


Figure 8.

Belova, Gorelenkov, Cheng

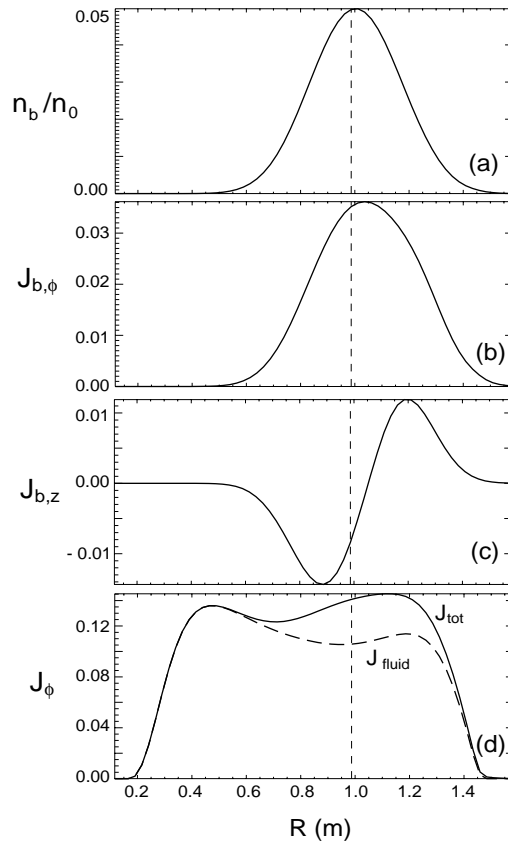


Figure 9.

Belova, Gorelenkov, Cheng

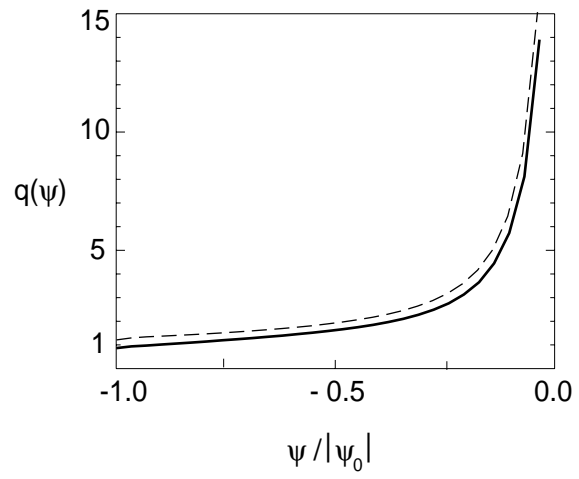


Figure 10.

Belova, Gorelenkov, Cheng

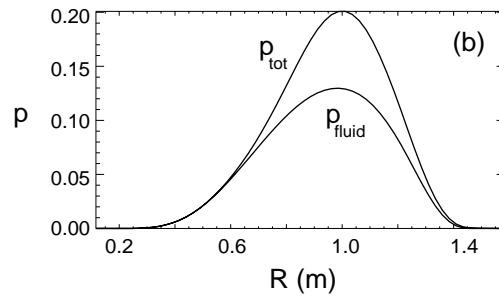
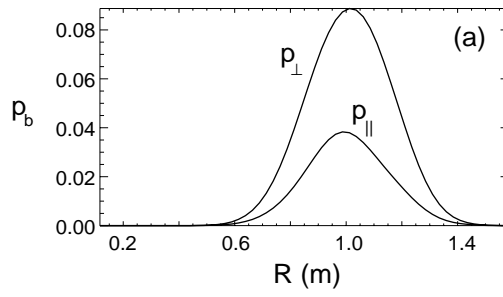


Figure 11.

Belova, Gorelenkov, Cheng

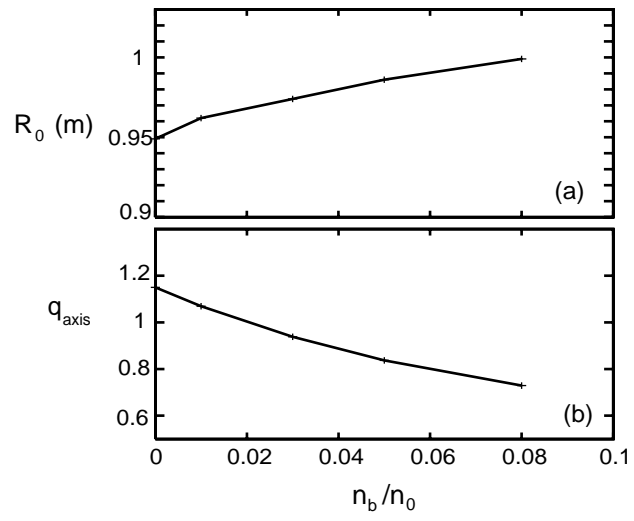


Figure 12.

Belova, Gorelenkov, Cheng

## External Distribution

Plasma Research Laboratory, Australian National University, Australia  
Professor I.R. Jones, Flinders University, Australia  
Professor João Canalle, Instituto de Fisica DEQ/IF - UERJ, Brazil  
Mr. Gerson O. Ludwig, Instituto Nacional de Pesquisas, Brazil  
Dr. P.H. Sakanaka, Instituto Fisica, Brazil  
The Librarian, Culham Laboratory, England  
Mrs. S.A. Hutchinson, JET Library, England  
Professor M.N. Bussac, Ecole Polytechnique, France  
Librarian, Max-Planck-Institut für Plasmaphysik, Germany  
Jolan Moldvai, Reports Library, MTA KFKI-ATKI, Hungary  
Dr. P. Kaw, Institute for Plasma Research, India  
Ms. P.J. Pathak, Librarian, Institute for Plasma Research, India  
Ms. Clelia De Palo, Associazione EURATOM-ENEA, Italy  
Dr. G. Grosso, Instituto di Fisica del Plasma, Italy  
Librarian, Naka Fusion Research Establishment, JAERI, Japan  
Library, Plasma Physics Laboratory, Kyoto University, Japan  
Research Information Center, National Institute for Fusion Science, Japan  
Dr. O. Mitarai, Kyushu Tokai University, Japan  
Dr. Jiangang Li, Institute of Plasma Physics, Chinese Academy of Sciences, People's Republic of China  
Professor Yuping Huo, School of Physical Science and Technology, People's Republic of China  
Library, Academia Sinica, Institute of Plasma Physics, People's Republic of China  
Librarian, Institute of Physics, Chinese Academy of Sciences, People's Republic of China  
Dr. S. Mirnov, TRINITI, Troitsk, Russian Federation, Russia  
Dr. V.S. Strelkov, Kurchatov Institute, Russian Federation, Russia  
Professor Peter Lukac, Katedra Fyziky Plazmy MFF UK, Mlynska dolina F-2, Komenskeho Univerzita, SK-842 15 Bratislava, Slovakia  
Dr. G.S. Lee, Korea Basic Science Institute, South Korea  
Institute for Plasma Research, University of Maryland, USA  
Librarian, Fusion Energy Division, Oak Ridge National Laboratory, USA  
Librarian, Institute of Fusion Studies, University of Texas, USA  
Librarian, Magnetic Fusion Program, Lawrence Livermore National Laboratory, USA  
Library, General Atomics, USA  
Plasma Physics Group, Fusion Energy Research Program, University of California at San Diego, USA  
Plasma Physics Library, Columbia University, USA  
Alkesh Punjabi, Center for Fusion Research and Training, Hampton University, USA  
Dr. W.M. Stacey, Fusion Research Center, Georgia Institute of Technology, USA  
Dr. John Willis, U.S. Department of Energy, Office of Fusion Energy Sciences, USA  
Mr. Paul H. Wright, Indianapolis, Indiana, USA

The Princeton Plasma Physics Laboratory is operated  
by Princeton University under contract  
with the U.S. Department of Energy.

Information Services  
Princeton Plasma Physics Laboratory  
P.O. Box 451  
Princeton, NJ 08543

Phone: 609-243-2750  
Fax: 609-243-2751  
e-mail: [pppl\\_info@pppl.gov](mailto:pppl_info@pppl.gov)  
Internet Address: <http://www.pppl.gov>